Supplementary Informations for

Cryo-EM structures reveal the electromotility mechanism of prestin, the cochlear amplifier

H. Futamata, M. Fukuda, R. Umeda, K. Yamashita, S. Takahashi, T. Shikakura, S. Hayashi, T. Nishizawa, K. Homma, O. Nureki.

Correspondence to: k-homma@northwestern.edu (K.H.), t-2438@bs.s.u-tokyo.ac.jp (T.N.) and nureki@bs.s.u-tokyo.ac.jp (O.N.)

This PDF file includes:

Supplementary Figs. 1 to 9
Supplementary Table 1
Captions for Supplementary Movies 1 and 2

Other Supplementary Materials for this manuscript include the following:

Supplementary Movies 1 and 2

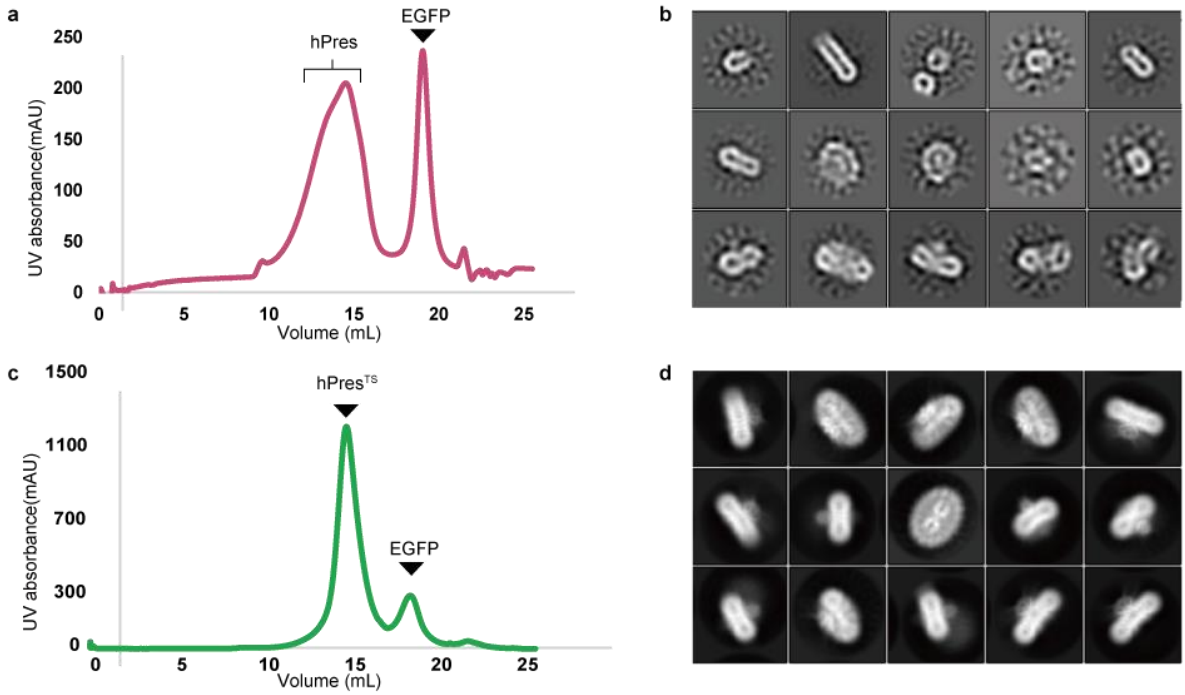

Supplementary Fig. 1. Purification of wild-type hPres and hPres^{TS}.

(a) A SEC profile for hPres. The elution fractions of hPres and EGFP are indicated. **(b)** Representative averaged 2D classes of wild-type hPres, indicating the high heterogeneity of the purified hPres protein. **(c)** SEC profile of hPres^{TS}. The elution fractions of hPres^{TS} and EGFP are indicated. **(d)** Representative averaged 2D classes of hPres^{TS}.

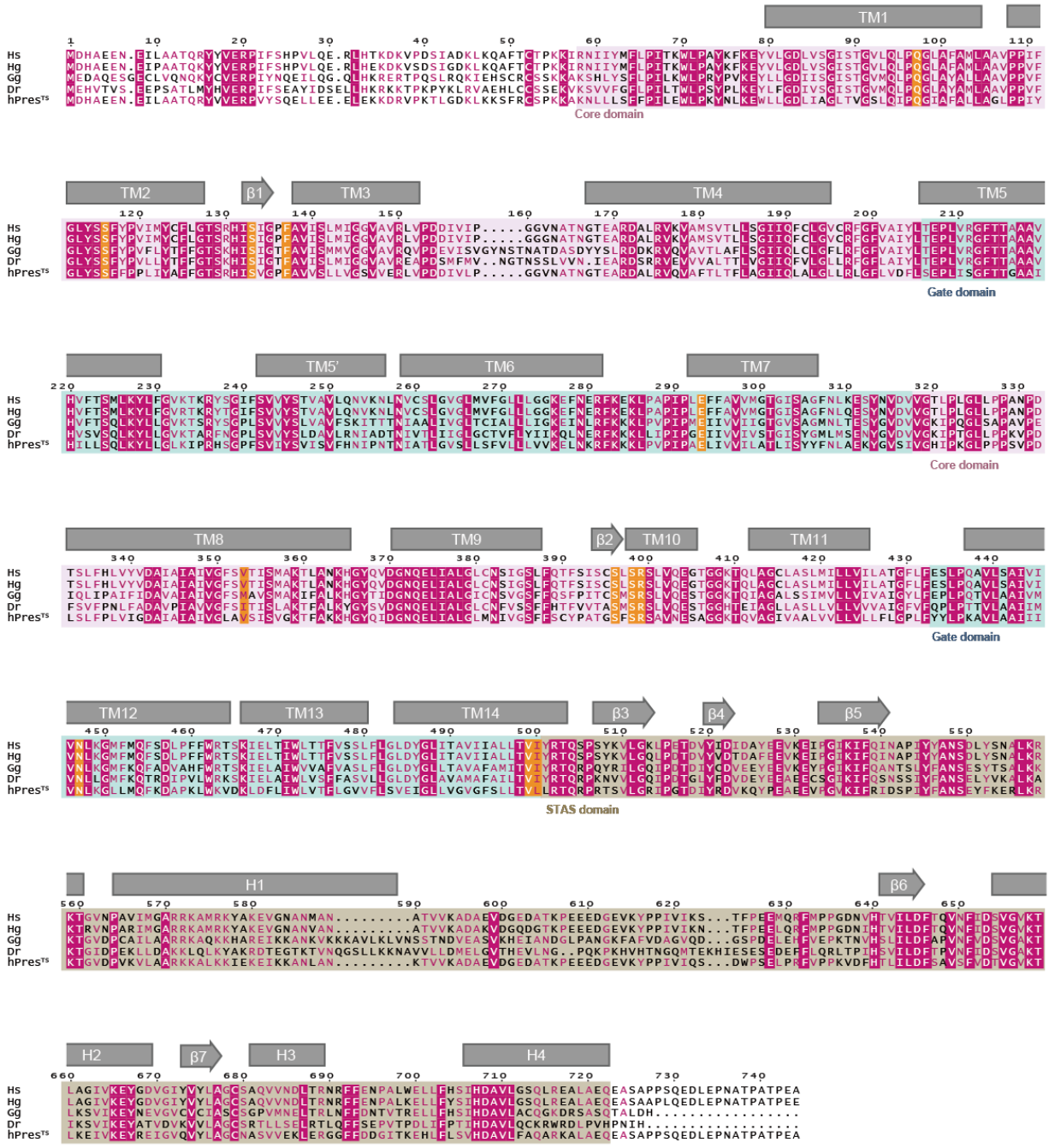

Supplementary Fig. 2. Sequence alignment of hPres^{TS} and prestin orthologs.

Sequence comparison of hPres^{TS} and four prestin orthologs (human (Hs), UniProt: P58743; naked mole rat (Hg), UniProt: G5BI49; chicken (Gg), UniProt: A0FKN5; zebrafish (Dr), UniProt: Q7T2N6). The locations of the transmembrane helices (TM), other α helices (H), and β strands (β) are also indicated. The residues contributing to the anion binding site, the core-gate domain interface, and the dimerization interface present in the transmembrane region are highlighted in orange.

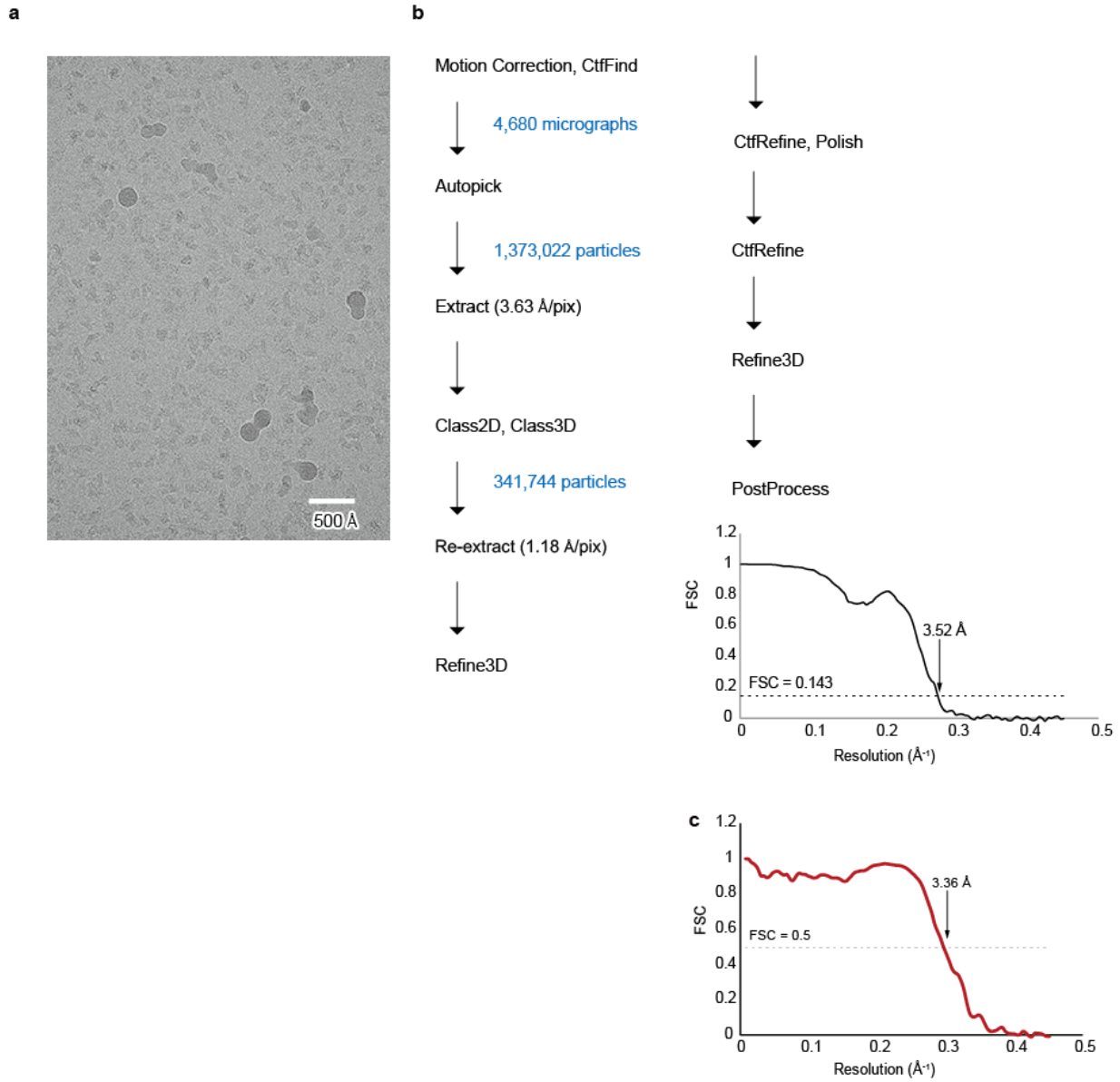

Supplementary Fig. 3. Data processing of the chloride-bound structure of hPres^{TS}

(a) Representative cryo-EM micrograph of the chloride-bound structure of hPres^{TS} in complex with chloride, recorded on a 300 kV Titan Krios electron microscope with a K3 camera. **(b)** Data processing workflow of the single particle image processing. Fourier Shell Correlation (FSC) between the two independently refined half-maps is shown. **(c)** FSC curves for map-to-model fitting.

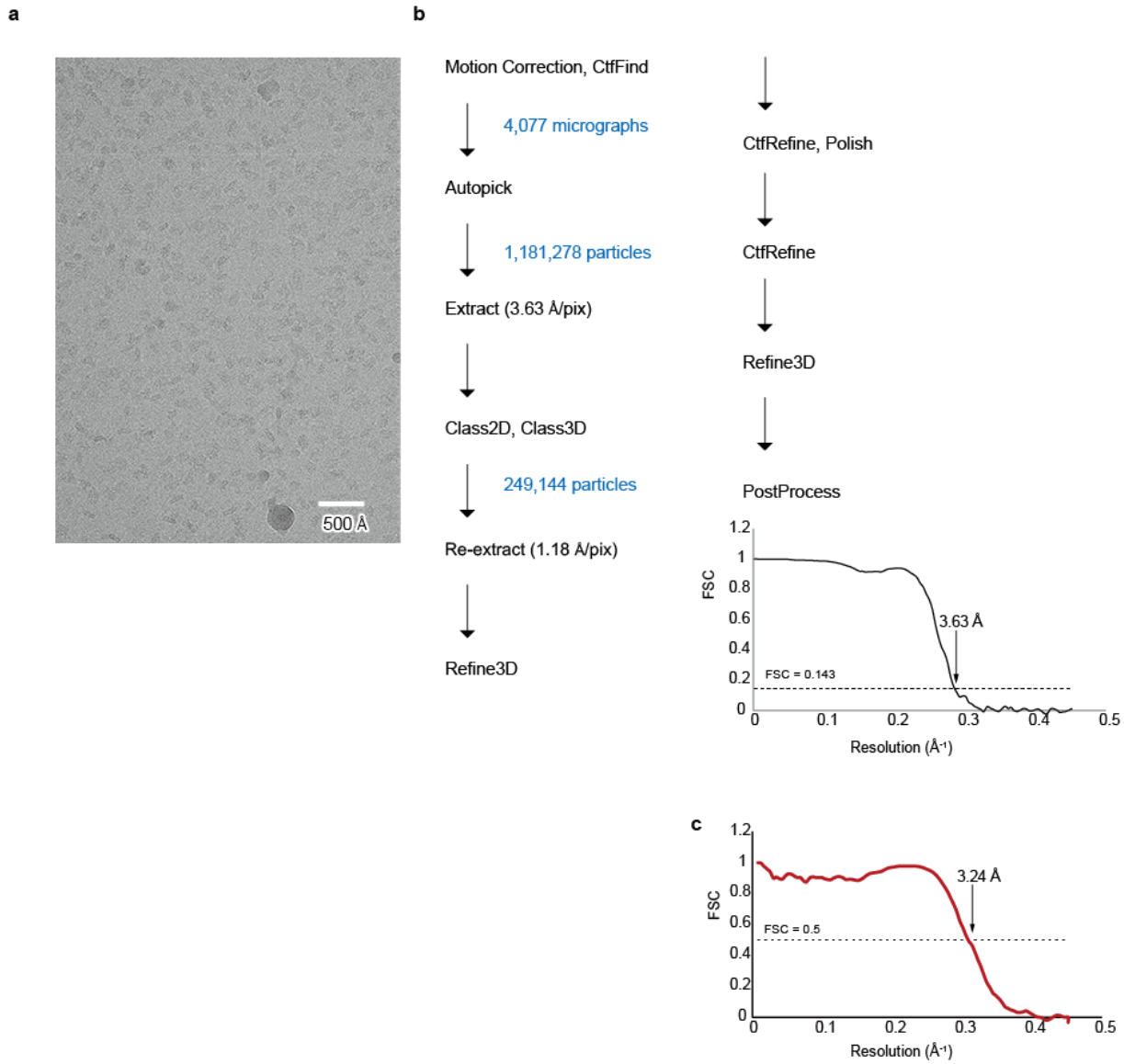

Supplementary Fig. 4. Data processing of the sulfate-bound structure of hPres^{TS}.
(a) Representative cryo-EM micrograph of the chloride-bound structure of hPres^{TS} in complex with sulfate, recorded on a 300 kV Titan Krios electron microscope with a K3 camera. **(b)** Data processing workflow of the single particle image processing. FSC between the two independently refined half-maps is shown. **(c)** FSC curves for map-to-model fitting.

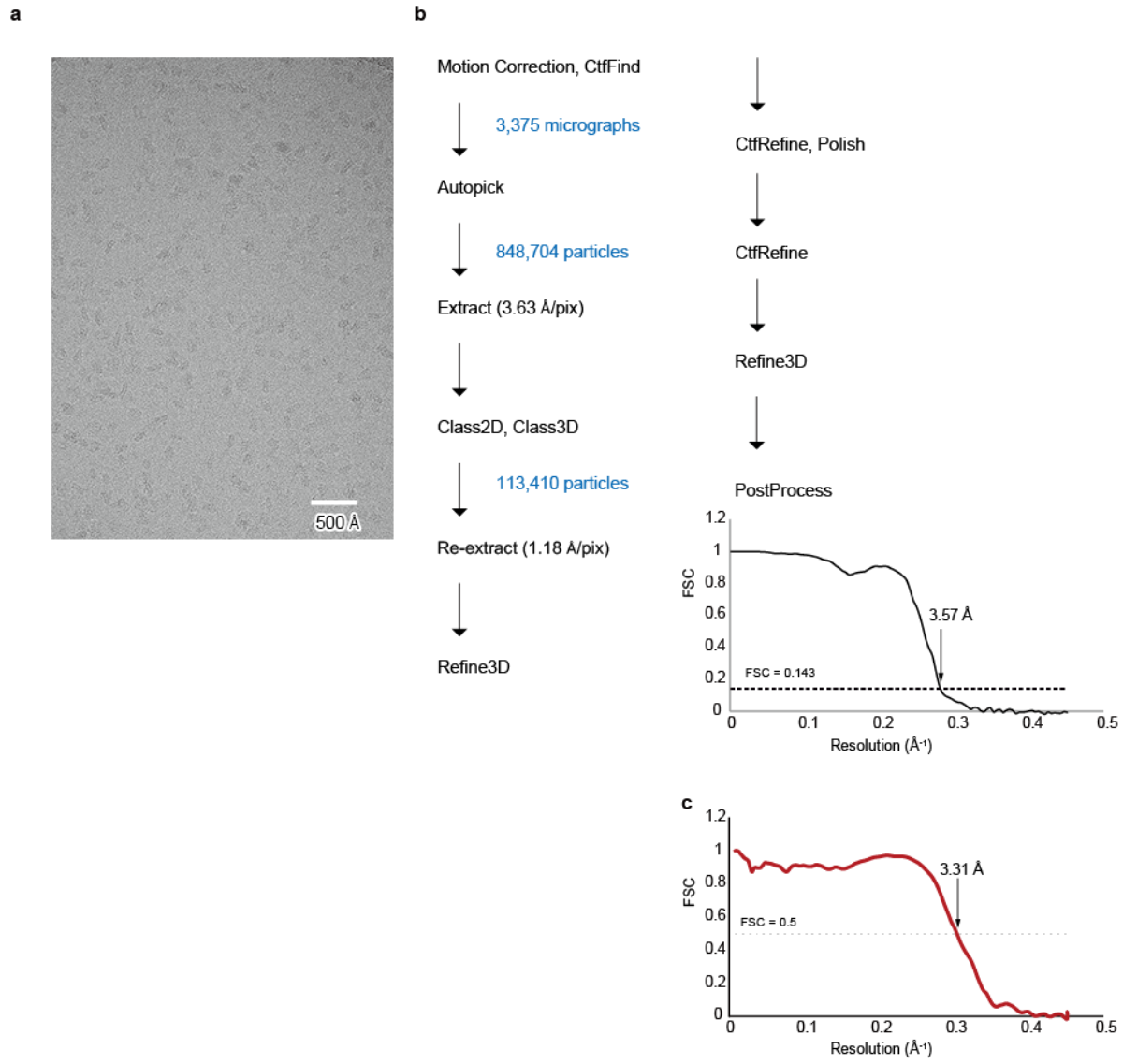

Supplementary Fig. 5. Data processing of the salicylate-bound structure of hPres^{TS}. **(a)** Representative cryo-EM micrograph of the chloride-bound structure of hPres^{TS} in complex with salicylate recorded on a 300 kV Titan Krios electron microscope with a K3 camera. **(b)** Data processing workflow of the single particle image processing. FSC between the two independently refined half-maps is shown. **(c)** FSC curves for map-to-model fitting.

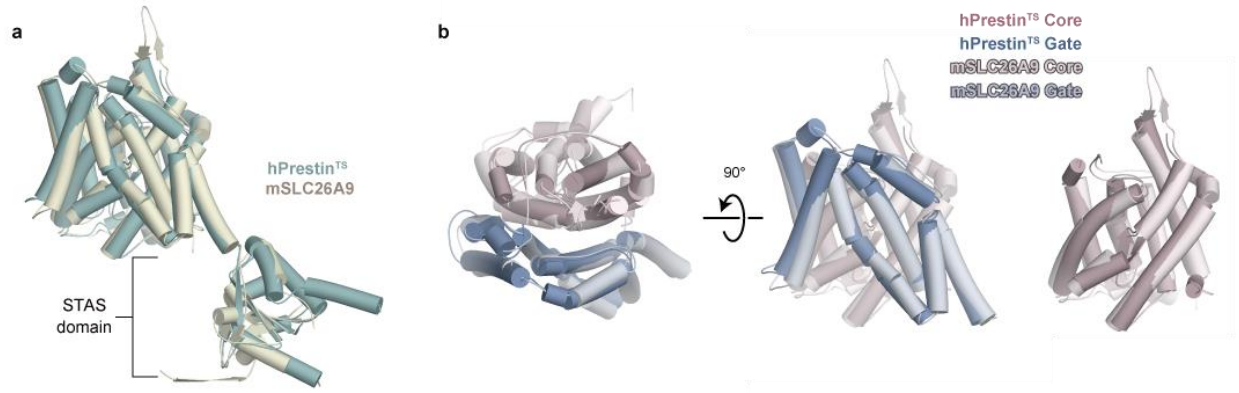

Supplementary Fig. 6. Structural comparison of hPres^{TS} and mSLC26A9.

(a) Structural superimposition of protomers of hPres^{TS} (green) and murine SLC26A9 (mSLC26A9) (PDBID: 6RTC, light beige). Both molecules are shown as cylinder models. Residues 58-722 of hPres^{TS} and 5-740 of murine SLC26A9 are superimposed together (R.m.s. deviation is 1.66 Å). **(b)** Structural superimposition of the transmembrane domains of hPres^{TS} (the same color scheme as in Fig. 1c) and the core (light pink) and gate (light blue) domains of murine SLC26A9 viewed from the extracellular side (left), the gate domain viewed from the lateral side (middle) and the core domain viewed from the lateral side (right).

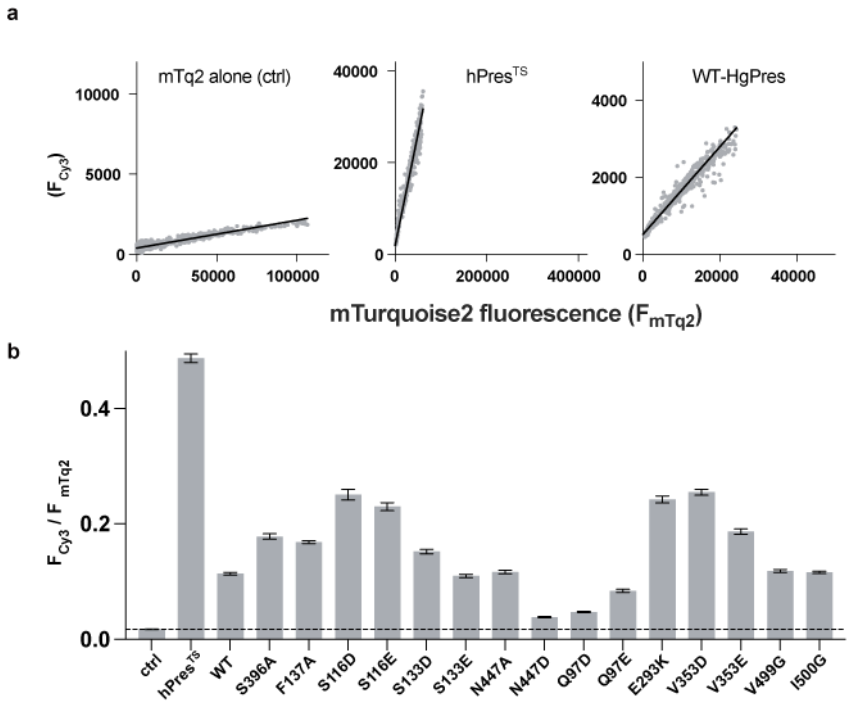

Supplementary Fig. 7. Quantification of membrane targeting efficiencies of the prestin constructs used in this study.

mTq2-tagged hPres^{TS} and HgPres constructs expressed in HEK293T cells were labeled with a membrane impermeable fluorescent probe, sulfo-Cy3 NHS ester. The cells were lysed, and the detergent extracted mTq2-tagged prestin proteins were captured by anti-mTq2 affinity beads. **(a)** Fluorescence intensities in the cyan (F_{mTq2}) and red (F_{Cy3}) channels were determined from images of the beads, and plotted against each other. Results for mTq2 alone (negative control), hPres^{TS}, and WT-HgPres are shown as examples. The X-Y axis ratio is fixed to 10 : 1. The slope (F_{Cy3}/F_{mTq2}) was determined by Deming's linear regression analysis, which indicates the efficiency of cell membrane targeting. **(b)** A summary of the cell membrane targeting efficiencies. Error bars indicate 95% confidence intervals of the slope values. The horizontal dashed line indicates the slope value of the negative control (ctrl).

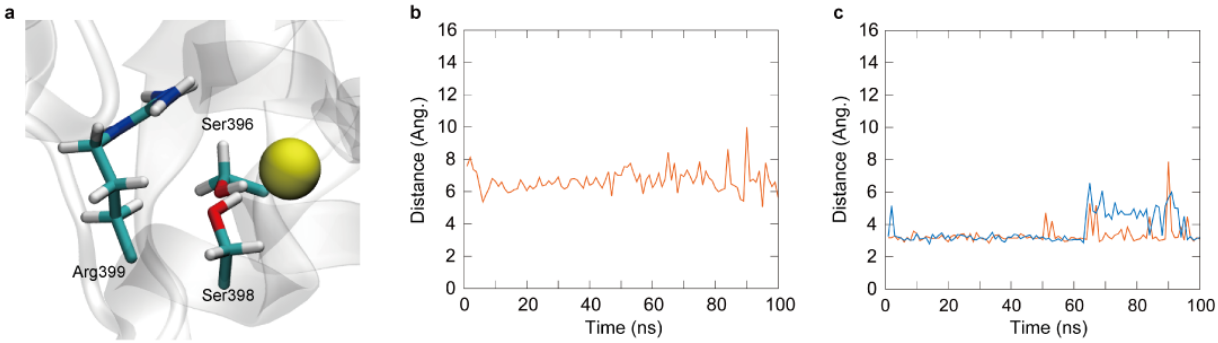

Supplementary Fig. 8. Structure and dynamics of chloride ion binding observed in MD simulations.

Cl^- binding in an MD simulation. A snapshot of the Cl^- binding **(a)** and time evolutions of the distances between Cl^- and C_ζ atom of Arg399 (**b**) and that between Cl^- and the O_ζ atoms of Ser396 (red) and Ser398 (blue) **(c)**, respectively, are depicted.

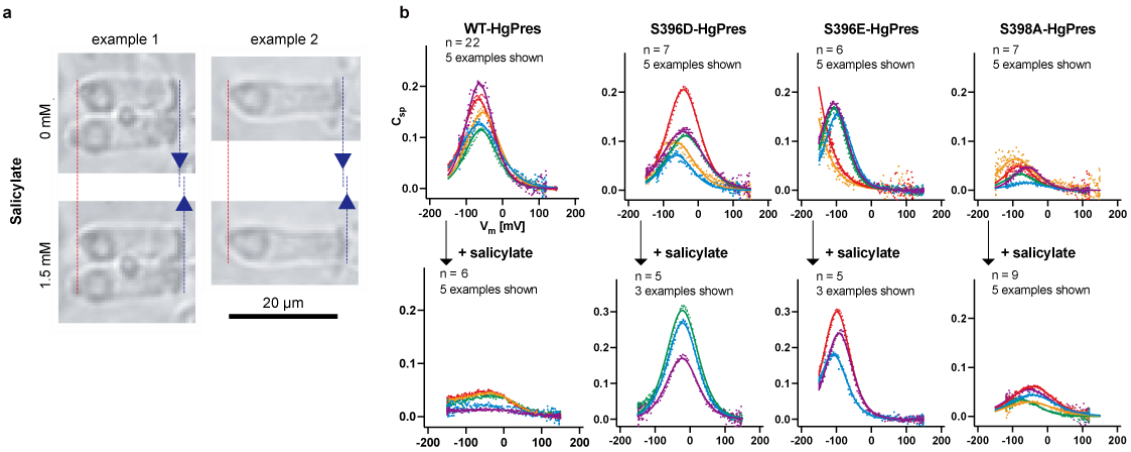

Supplementary Fig. 9. The effects of salicylate on wild-type OHCs and HEK cells expressing various HgPres constructs.

(**a)** Salicylate-induced elongation of OHCs. Video frame images of OHCs before (upper panels) and after (bottom panels) the application of 1.5 mM salicylate in the bath solution (see also Supplementary Movie 2). **(b)** The effect of salicylate on the NLC of WT-, S396D-, S396E-, and S398A-HgPres. NLC was measured in the absence (upper panels) and presence (lower panels) of 10 mM salicylate in the bath solution. Three to five examples are shown in different colors for each construct and condition.

Data collectioin and processing			
EMDB-ID	31757	31758	31759
PDB ID	7V73	7V74	7V75
Bound anion	Chloride	Sulfate	Salicylate
Microscope	Titan Krios G4		
Detector	Gatan K3 Camera with Quantum LS energy filter		
Magnification	105,000		
Voltage (kV)	300		
Electron exposure (e^{-}/Å^2)	54	54	54
Defocus range (μm)	-0.8 to -1.6		
Pixel size (Å/px)	0.83		
Symmetry imposed	C2		
Number of movies	4,680	4,077	3,375
Initial particle images	1,373,022	1,181,278	848,704
Final particle images	341,744	249,144	113,410
Map resolution (Å)	3.52	3.63	3.57
FSC threshold	0.143		
Map sharpening B factor (Å^2)	-188.514	-181.17	-171.721
Model building and refinement			
Model composition			
Protein atoms	4620	4620	4687
Metals	0	0	0
Other atoms	252	249	299
R.M.S. deviations from ideal			
Bond lengths (Å)	0.0107	0.0125	0.012
Bond angles (°)	1.697	1.8889	1.7164
Validation			
Clashscore	5.78	4.26	6.41
Rotamer outliers (%)	1.99	3.38	5.68
Ramachandran plot			
Favored (%)	95.26	93.23	94.66
Allowed (%)	4.74	6.6	5.18
Outlier (%)	0	0.17	0.17

Supplementary Table 1. Data collection, processing, model refinement and validation. Clashscores, rotamer outliers, and Ramachandran plots were calculated using MolProbity [62].

Supplementary Movie 1. Rigid-body domain movement deduced from the chloride- vs. salicylate-bound hPres^{TS} structures.

The salicylate-bound and chloride-bound structures are overlayed with the gate domains used as superimposition references. The anion binding site is indicated by a circle. See also Fig. 3C.

Supplementary Movie 2. Salicylate-induced elongation of mouse OHCs.

Salicylate (1.5 mM) was added to the bath solution at time zero.